RSC Advances

PAPER

Cite this: *RSC Adv.*, 2015, **5**, 55109

Eco-friendly synthesis of hierarchical ginkgo-derived carbon nanoparticles/NiAl-layered double hydroxide hybrid electrodes toward high-performance supercapacitors†

Mingkai Liu,[ab] Sixin He,[a] Yue-E Miao,[a] Yunpeng Huang,[a] Hengyi Lu,[a] Longsheng Zhang[a] and Tianxi Liu*[ab]

Received 21st April 2015
Accepted 16th June 2015

DOI: 10.1039/c5ra07215h

www.rsc.org/advances

Three-dimensional carbon nanoparticles (CPs)/Ni–Al layered double hydroxide (NiAl-LDH) (CP/LDH) hybrids with hierarchical nanostructures have been facilely prepared with NiAl-LDH nanosheets homogeneously located on the surface of CPs through an *in situ* hydrothermal growth process. Eco-friendly synthesized from the fallen ginkgo leaves, CPs with mesoporous architecture are chemically activated and used as building blocks for the construction of hierarchical CP/LDH hybrids. Mesoporous CPs coupled with the NiAl-LDH nanosheets are favorable to improve the mass transfer, adsorption/desorption of ions, as well as the electrochemical performance of the electrodes. The electrochemical measurements show that CP/LDH hybrid exhibits a remarkably enhanced specific capacitance of 1355 F g^{-1} at 5 mV s^{-1}, compared with 121 F g^{-1} of CPs and 405 F g^{-1} of pure NiAl-LDHs, as a result of the synergistic effect from electrochemical double layer capacitance of CPs and pseudocapacitance of NiAl-LDHs. Furthermore, the CP/LDH hybrid shows excellent rate capability and good long-term cycling performance with 90% capacitance retained after 2000 cycles. Therefore, the facilely prepared CP/LDH hybrids are promising electrode materials for potential applications in energy storage devices.

1. Introduction

Electrochemical capacitors, also called supercapacitors, have attracted tremendous interest and become one of the most popular research hotspots due to their outstanding abilities of storing large amounts of energy and transporting high power loads within a short time.[1–4] Generally, supercapacitors can be divided into two categories according to their charge storage mechanisms: (i) electrochemical double layer capacitors (EDLCs), based on ion adsorption process, and (ii) pseudo-capacitors, *via* fast surface redox reactions.[5–7] The most used active electrode materials include carbon-based nanomaterials for EDLCs, and electrically conductive polymers as well as transition metal (Ni, Mn, Co, *etc.*) oxides and hydroxides for pseudo-capacitors.[8,9] It should be noted that, the performance of supercapacitors is greatly dependent on the properties of active electrode materials. Therefore, superior electrode materials with high specific surface area, good pore volume and large number of active sites are urgently needed for developing new generation energy-storage systems.[10–14]

Carbon nanomaterials including carbon nanotubes, carbon nanofibers, and graphene sheets, have been identified as the most preferable materials for EDLC electrode due to their unique features of electrical conductivity, high surface area, strong mechanical strength, environmental friendliness, as well as low cost characteristic. Taking graphene as example, the specific surface area of isolated graphene sheets is about 2600 m^2 g^{-1}, and its theoretical can reach 550 F g^{-1}.[15] However, the restacking and aggregation of graphene sheets and carbon nanotubes due to the strong van der Waals interaction among the neighboring layers lead to the heavy reduction of their electrochemical properties. To date, activated carbon nanomaterials have become hot topics for their excellent chemical and physical properties, especially under the rapid depletion of fossil fuels such as coal, oil and gas.[16–20] Recently, activated carbons have been utilized in a wide range of applications such as air purification, chemicals removal, solvents recovery, molecular serving, and treatment of products in chemical industries for their unique properties of low cost, availability, high surface area, as well as other characteristics.[21,22] Generally, the activated carbons are prepared

[a]*State Key Laboratory of Molecular Engineering of Polymers, Department of Macromolecular Science and Laboratory of Advanced Materials, Fudan University, Shanghai, 200433, P. R. China. E-mail: txliu@fudan.edu.cn; Fax: +86-21-65640293; Tel: +86-21-55664197*

[b]*School of Chemistry and Chemical Engineering and Jiangsu Key Laboratory of Green Synthetic Chemistry for Functional Materials, Jiangsu Normal University, Xuzhou 221116, P. R. China*

† Electronic supplementary information (ESI) available. See DOI: 10.1039/c5ra07215h

from coal and other dense plant materials such as wood and nut shells.[23] It is worthy to mention that biomass is considered as one of the natural and renewable sources for eco-friendly preparation of activated carbons.[24] To date, several porous activated carbon materials with unique EDLC properties have been designed and synthesized from "natural waste" biomaterials. Functional conducting carbon materials with a high specific surface area of 1230 $m^2\ g^{-1}$ have been synthesized from plant leaves through a single-step pyrolysis treatment, resulting in a high specific capacitance of 400 F g^{-1}.[25] Also, Zhang *et al.* have successfully prepared activated porous carbon materials from biomass waste of various pollens through a green and low-cost chemical activation method, achieving the formation of high-performance electrode materials with a high specific surface area up to 3037 $m^2\ g^{-1}$ and capacitance of 207 F g^{-1}.[26]

Layered double hydroxides (LDHs), are a class of lamellar compounds with a general chemical formula of $[M^{II}_{1-x}M^{III}_x(OH)_2]^{x+}[A^{n-}]_{x/n}\cdot mH_2O$, where M^{II} and M^{III} are divalent and trivalent cations respectively, and A^{n-} is *n*-valent interlayer guest anion.[27–29] LDH-based nanomaterials have been widely used in numerous applications for their unique characteristics such as high redox activities, environmentally friendly nature, and relatively low cost.[30–32] To date, LDHs have been reported to be promising supercapacitor electrode materials with fast ion/electron transfer and good electrochemical activities resulted from their high surface areas and a large number of electrochemical active sites.[33–35]

However, electrodes prepared by simply utilizing carbon materials or functional pseudo capacitance materials alone cannot meet the needs of practical applications in supercapacitors, such as ultrahigh specific capacitance (for carbon materials) as well as long cycle durability (for pseudo capacitance materials).[12,13,17] Hybrid nanomaterials used for high performance electrodes by combining carbon nanomaterials with EDLC performance and LDH nanomaterials with pseudo capacitance can be an effective way to greatly improve the existing problems for both carbon materials and LDHs.[21,30]

Here, a simple but effective method has been presented for preparing carbon nanoparticles (CP) from biomass waste of fallen ginkgo leaves through hydrothermal and chemical activation treatments. The obtained CP materials with average diameters of 50–200 nm show high specific surface area of 761 $m^2\ g^{-1}$ without apparent aggregation or restacking. NiAl-LDH nanosheets were uniformly grown on the surface of CPs, achieving the formation of hierarchically structured hybrid materials of CPs and NiAl-LDHs (CP/LDH). The hybrid CP/LDH materials exhibit higher specific capacitance of 1355 F g^{-1} than those of pristine CP materials (121 F g^{-1}) and pure NiAl-LDHs (405 F g^{-1}) at a scan rate of 5 mV s^{-1}. Moreover, the CP/LDH hybrids show excellent cycling stability with 90% specific capacitance maintained after 2000 cycles. These remarkable performances of CP/LDH hybrids have adequately confirmed the successful hybridization of CPs and NiAl-LDH nanosheets, and achieved the synergistic effect of EDLC and pseudocapacitance property respectively from CPs and NiAl-LDH nanosheets.

2. Experimental section

2.1 Materials

Ginkgo leaves were collected in the campus of Fudan University, Shanghai, China. Concentrated sulfuric acid (H_2SO_4, 98 wt%), potassium permanganate ($KMnO_4$), hydrogen peroxide (H_2O_2, 30 wt%), nickel(II) nitrate hexahydrate ($Ni(NO_3)_2\cdot 6H_2O$), aluminum isopropoxide ($Al(OPr)_3$), potassium hydroxide (KOH), urea were purchased from China Medicine Co. Ltd. Autoclaves (50 mL and 100 mL) were provided by Shanghai to the China Instrument and Equipment Co. Ltd. All reactants were of analytical purity and used directly without any further purification. Ultraclean water was used throughout the experiments.

2.2 Preparation of carbon nanoparticles

The carbon nanoparticles (CPs) were prepared from ginkgo leaves. Firstly, the ginkgo leaves were washed with ultraclean water and dried at 70 °C for 5 h. Small slices of these ginkgo leaves were high-temperature carbonized at 900 °C for 6 h in argon atmosphere. Then, the carbonized ginkgo leaves were mechanically milled, resulting in the formation of powdery carbon materials. Thus obtained powdery carbon materials were further treated by an industry KOH activation step. Briefly, powdery carbon product was fully mixed with 4 times weight of KOH and heated at 900 °C for 90 min at argon atmosphere. The obtained powdery product was washed with 0.1 M HCl and ultraclean water respectively for 5 times to remove any residual salts before being dried at 120 °C for 10 h, resulting in the formation of CP materials.

2.3 Fabrication of CP/LDH hybrids

Fig. 1 schematically illustrates the fabrication process of CP/LDH hybrids. Here, Boehmite (AlOOH) was used as the precursor for preparing NiAl-LDH nanosheets.[36,37] Briefly, 11.3 g of $Al(OPr)_3$ was dissolved into 100 mL of ultraclean water by stirring at 85 °C until a transparent solution was formed. HNO_3 solution (1 M) was progressively added into the solution for hydrolysis of $Al(OPr)_3$, with pH value of the solution held in the range of 3–4. The solution was stirred at 85 °C for 2 h before being slowly cooled to room temperature. AlOOH solid was obtained after evaporation of water in the solution and mechanically milled to achieve powdery AlOOH particles. 5.4 g of this AlOOH solid material was dissolved into 100 mL ultraclean water by stirring at 85 °C for 1 h. Then, HNO_3 solution (9.3 mL, 1 M) was added to the solution and refluxed gently for 6 h. After being cooled to room temperature, the AlOOH primer sol was obtained.

CP/LDH hybrids with different contents of NiAl-LDH nanosheets were prepared through a hydrothermal process. Typically, 10 g of CP material was dissolved into 30 mL of ultraclean water, and 2 mL of AlOOH sol, 0.218 g of $Ni(NO_3)_2$ and 0.15 g of urea were added into the mixture under ultrasonication and vigorous stirring. The mixed solution was transferred into a sealed autoclave (100 mL) and heated at 100 °C for 24 h. Finally, the obtained product was washed with ultraclean water and ethanol for several times and dried at 70 °C for 12 h to obtain

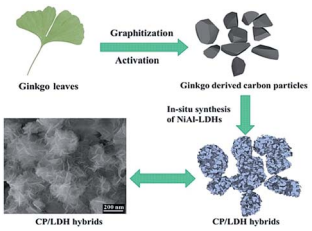

Fig. 1 Schematic illustration of the formation process of CP/LDH hybrids.

CP/LDH hybrids. Here, the amount of AlOOH, $Ni(NO_3)_2$ and urea were gradually increased by 3, 5, and 7 times in order to prepare CP/LDH hybrids with different contents (*i.e.*, 8, 19, 29, and 37 wt%) of NiAl-LDH nanosheets which are respectively denoted as CP/LDH-1, CP/LDH-3, CP/LDH-5 and CP/LDH-7.

2.4 Characterization

X-ray diffraction (XRD) patterns were conducted on a Bruker GADDS X-ray diffractometer using Cu Ka radiation under a current of 40 mA and a voltage of 40 kV. Field-emission scanning electron microscope (FESEM) characterizations were performed on Ultra 55 (Zeiss, Germany) with an accelerating voltage of 20 kV, and the corresponding energy-dispersive spectroscopy (EDS, X-Max 50, Oxford instrument) spectra were also collected to study the morphologies of the samples. Raman spectra were recorded on a Laser Raman spectrometer (XploRA, HORIBA JobinYvon) based on a He–Ne laser (λ = 632.8 nm). Surface area measurements were obtained by the Brunauer–Emmett–Teller (BET) method, which were carried out according to the physical adsorption of N_2 at 77 K using Autosorb-1 Quantachrome Instruments. Metal ions content analysis was performed on inductively coupled plasma instrument (P-4010, Hitachi). Specifically, 10 mg of sample CP/LDH-5 was boiled in nitric acid solution (10 wt%) for 1 h, and the obtained supernatant liquid was further used for the ICP analysis.

2.5 Electrochemical measurements

Electrochemical characterizations were carried out on a CHI-660D electrochemical workstation (Shanghai Chenhua, China). The electrochemical performances of the obtained CP, LDH, CP-LDH products were investigated based on a three-electrode testing system. Briefly, the as-obtained active material, acetylene black, and polytetrafluoroethylene (PTFE) were mixed with a mass ratio of 80 : 15 : 5, and then dispersed in isopropanol to yield a homogeneous paste. Then, the resulting slurry (with 2 mg of the active material) was coated onto a nickel foam substrate (40 × 10 × 1 mm^3) and dried at 80 °C for 12 h, followed by being compressed at 1.5 MPa to obtain the working electrode. Finally, the electrochemical properties were evaluated by cyclic voltammetry (CV) tests (0.0–0.5 V, 5–100 mV s^{-1}), galvanostatic charge–discharge tests, electrochemical impedance spectroscopy (EIS), as well as cycle stability in 6 mol L^{-1} KOH aqueous solution at room temperature with a saturated calomel electrode (SCE) as the reference electrode and a Pt foil as the counter electrode. The specific capacitance values were calculated according to the CV curves with the following equation:

$$C_{sp} = \frac{\int I \cdot dv}{v \cdot m \cdot \Delta V} \quad (1)$$

in which, C_{sp} (F g^{-1}) is the total specific capacitance of the active electrode materials, I is the oxidation or reduction current intensity (A), v is the scan rate (mV s^{-1}), ΔV is the potential window of the CV curves (V), and m is the mass of active materials (g).

3. Results and discussion

3.1 Morphology and structure of CPs and CP/LDH hybrids

The CP materials used in this work were prepared by carbonization of ginkgo leaves. As seen in Fig. 2a, the carbonized material can still keep the sheet-structure of ginkgo leaves while ginkgo-derived CP powders can be achieved after being milled (Fig. 2b). In order to increase the porosity and specific surface area, the CP powders were further actively treated with KOH, thus resulting in the activated CP nanoparticles which can be homogeneously dispersed in DMF (Fig. 2c). Fig. 2d and e show the low and high magnification SEM images of CP materials after being treated by milling and KOH activation. Small CP nanoparticles with diameters of 20–200 nm as well as sharp corners can be clearly observed. Moreover, they can be uniformly dispersed without serious aggregation, which can effectively promote the efficient deposition of functional NiAl-LDHs on their surface. Thus eco-friendly prepared CP nanoparticles with nanoscale size can achieve a high specific surface area and mesoporous structure after chemical activation, which can efficiently enhance the electrochemical performance of CP nanoparticles by shorting the diffusion length of electrolyte.

The specific surface area and pore size distribution of the prepared CP nanoparticles have been characterized according to BET method (Fig. 3). Based on IUPAC data classification, the nitrogen adsorption–desorption isotherm of CP nanomaterial is

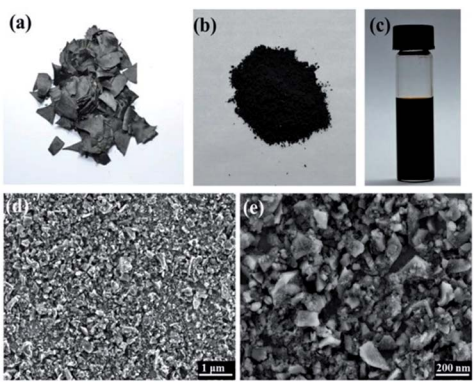

Fig. 2 Digital images showing carbonized ginkgo leaves (a), ginkgo-derived CP powder treated by mechanical milling (b), dispersion of CP nanoparticles in DMF (c), and SEM images of CP nanoparticle with low (d) and high (e) magnifications.

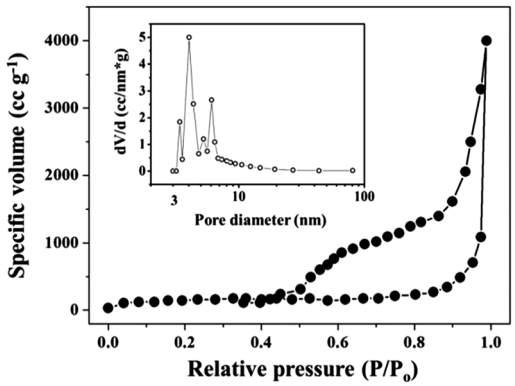

Fig. 3 Nitrogen adsorption–desorption isotherm and the BJH adsorption pore size distribution (inset) of CP materials at 77 K.

of typical IV pattern with a sharp capillary condensation step at high relative pressures, which is a characteristic hysteresis loop of asymmetric, slit-shaped mesoporous materials.[38] The hysteresis loop in the low relative pressure (P/P_o) range between 0.50 and 0.90 indicates the presence of mesoporous structure,[8] thus resulting in the well-developed porosity of CP materials with uniform pore size distribution around 3–7 nm and a high specific surface area of 761 $m^2\ g^{-1}$, which is much higher than the untreated CP materials with 126 $m^2\ g^{-1}$, as seen in Fig. S1.† The excellent porous structure can be ascribed to the activation effect of KOH, where chemical reaction between KOH and carbon atom happens under temperature higher than 700 °C:[7,39,40]

$$2C + 6KOH \rightarrow 2K + 3H_2 + 2K_2CO_3 \quad (2)$$

and subsequent decomposition of K_2CO_3 and/or reactions of $K/K_2CO_3/CO_2$ with the carbon atom gives the loss of carbon, resulting in the generation of large amount of nanoscale pores in the obtained CP nanomaterial. Thus, the high specific surface area and excellent mesoporous structure of CP nanomaterial can endow themself with high electrochemical capacity by giving the possibility of efficient transport of ions and electrons.

The porous CP materials derived from ginkgo leaves were further used as carbon substrate for preparation of CP/LDH hybrids. As seen in Fig. 4a, NiAl-LDH nanosheets were homogeneously grown on the surface of CPs with close contacting while the edges and corners of CPs can still be clearly observed (as indicated by the arrows) for CP/LDH-1 with low content (8 wt%) of NiAl-LDH nanosheets. This close interfacial contacting can be ascribed to the strong electrostatic interaction between positively charged NiAl-LDHs and negatively charged CPs.[41,42] Furthermore, it can be clearly seen that the NiAl-LDH grown on the surface of CPs existed as layered morphology with good porous structure (Fig. 4b). These layered NiAl-LDH nanosheets with porous structure can promote the rapid transfer of electrolyte ion and facilitate the utilization of the mesopores of CPs. With the content of NiAl-LDH increasing, CP/LDH-5 hybrids with sphere-like morphology were obtained due to the layer-by-layer deposition of NiAl-LDH nanosheets (as seen in Fig. 4c). Here, the CPs with mesoporous structure can play an important role in promoting the homogenous deposition of NiAl-LDHs by tightly contacting with functional NiAl-LDH nanosheets. Moreover, with CPs acting as the skeletons, the obtained CP/LDH-5 hybrids with open frameworks can provide more exposed electrochemically active sites than the aggregated pure NiAl-LDHs (Fig. 4d), which can accelerate the full utilization of electrochemically active NiAl-LDH nanosheets. With further increasing the content of NiAl-LDH, cactus-liked CP/LDH-7 with redundant NiAl-LDH nanosheets was prepared, as seen in Fig. 5. The high content of NiAl-LDHs (37 wt%) have totally overlapped the exposed surface of CPs, and especially impeded the usage of the porous structure of CP materials, which may severely affect the electrochemical performance.

The successful deposition of NiAl-LDHs on the surface of CPs was further confirmed by EDS elemental mapping. Fig. 6 shows a SEM image of CP/LDH-5 hybrids combined with EDS mapping images made from K-line energy densities of C, Al, Ni, O as well as Si. The Si element mapping can be ascribed to the Si wafer for loading the CP/LDH-5 sample, and the relative lower intensity of C mapping can be ascribed to the overlapping effect of the outer layer NiAl-LDHs. Compared to the C mapping, the Al, Ni and O mappings with strong distribution intensity are clearly noticeable, which further indicates the successful and homogenous deposition of NiAl-LDH nanosheets on CPs. In addition, the uniform distribution and tight adhesion of NiAl-LDHs can be beneficial for the synergistic effect of CPs and NiAl-LDH nanosheets in electrochemical applications.

The crystal structures of CP, CP/LDH hybrids, as well as pure NiAl-LDH spheres were investigated by XRD characterization (Fig. 7). The XRD pattern of CP material shows a board diffraction peak at about 26.1° similar to those of biomaterial-derived carbon materials,[43,44] which can be assigned to the (002) crystal planes of the activated CPs with good oriented aromatic carbon sheets.[45] The characteristic diffraction peak of CP materials also can be observed in the XRD pattern of CP/LDH-1 hybrids due to the low content of NiAl-LDHs. Interestingly, the characteristic diffraction peaks of NiAl-LDHs were gradually became apparent and sharp with the content of NiAl-LDH nanosheets increasing, which corresponds to the 003, 006, 012 and 018 planes of NiAl-LDH. The consistent XRD patterns of CP/LDH-3, CP/LDH-5 and CP/LDH-7 composites with that of pure NiAl-LDH spheres indicate that the presence of CP materials does not influence the crystal structure of the deposited NiAl-LDH sheets. However, CP supported NiAl-LDH sheets exhibit weaker and boarder Bragg reflections, which can be ascribed to the polar surface of CP materials that may affect the ordered stacking of NiAl-LDH sheets through electrostatic interactions.[36]

The interactions between CP materials and NiAl-LDH nanosheets were further investigated by Raman spectroscopy, as shown in Fig. 8. For CP nanoparticles, D band at 1341 cm^{-1} from the breathing mode of point photons of A1g symmetry and G band at 1571 cm^{-1} presenting the first order scattering of the E_{1g} phonon for sp^2 C atoms are clearly observed, indicating the carbonic nature of CP nanoparticles.[46] Raman spectra of

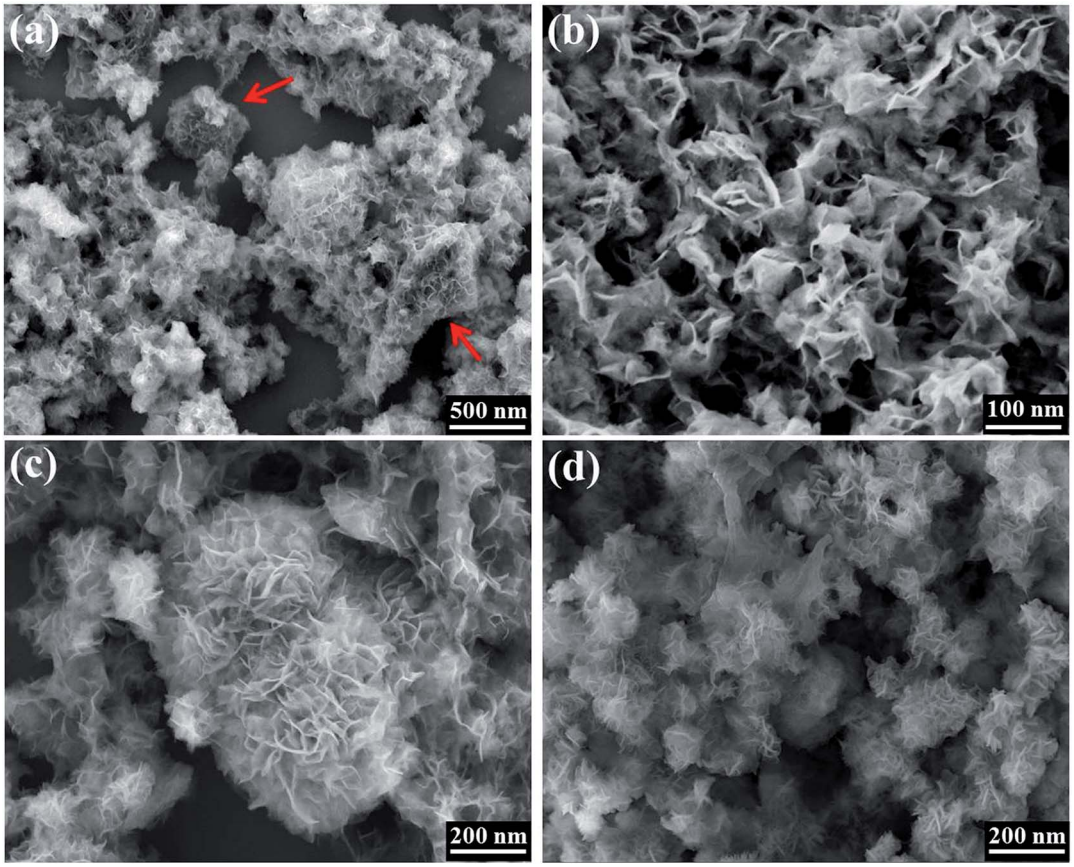

Fig. 4 SEM images of CP/LDH-1 composite with low and high magnifications (a and b), CP/LDH-5 (c), as well as the pure NiAl-LDH sphere (d).

NiAl-LDH shows two obvious characteristic peaks located at 546 cm^{-1} and 1058 cm^{-1}, which can be typically assigned to Ni–Al based LDHs.[47] The CP/LDH composites exhibit both the characteristic Raman breathing peaks of carbon nanomaterials and NiAl-LDHs, confirming the successful hybridization of CP materials and NiAl-LDHs. Furthermore, the relative intensity of Raman peaks of NiAl-LDHs in the CP/LDH composites was gradually increased with the NiAl-LDHs contents increasing, which is consistent with the morphology from the FESEM images (Fig. 4 and 5).

3.2 Electrochemical performance of CPs, pure NiAl-LDHs, and CP/LDH hybrids

The layered NiAl-LDH nanosheets located on the surface of CP materials create a hierarchical porous structure of CP/LDH materials, which is the ideal morphological foundation for their fast redox reactions with the electrolyte. The potential applications of the prepared CP materials, pure NiAl-LDH spheres, and CP/LDH hybrids in supercapacitors have been investigated by CV, EIS, and galvanostatic charge–discharge measurements in electrolyte of 6 mol L^{-1} KOH solution. Fig. 9a shows the CV curves for all the prepared materials at scan rate of 20 mV s^{-1}. The rectangular CV curve of CP material can be ascribed to its typical EDLC performance,[48] while pure NiAl-LDH sphere exhibits a pair of redox peaks indicating the pseudo-capacitance.[32] These two redox peaks can be attributed to the redox of Ni^{2+}/Ni^{3+} with OH^- by the following equation:

$$Ni(OH)_2 + OH^- \leftrightarrow NiOOH + H_2O + e^- \quad (3)$$

CP/LDH samples exhibit similar redox peaks with higher redox current densities, confirming the successful hybridization of NiAl-LDH nanosheets and CP materials. Since the specific capacitance is proportional to the area surrounded by the CV curves,[13,49] capacitance measurements based on the surrounded area of CV curves according to eqn (1) show that CP/LDH-5 has the largest specific capacitance of 1355 F g^{-1} at scan rate of 5 mV s^{-1}, which can be also proved by its longest charge–discharge time (as seen in Fig. 9b). Compared with the specific capacitance of pristine CP materials (121 F g^{-1} at 5 mV s^{-1}) and pure NiAl-LDH spheres (405 F g^{-1} at 5 mV s^{-1}), the greatly enhanced specific capacitance of CP/LDH-5 can be attributed to the synergistic effect of good pseudo-capacitance of NiAl-LDH nanosheets and the large surface area of CP materials derived from the activated effect of KOH accessible for electrolyte ion transport.

Furthermore, CV curves of CP/LDH-5 electrode at various scan rates between 5 to 100 mV s^{-1} are shown in Fig. 9c. It is obvious that each curve at different scan rates shows similar anodic and cathodic peaks, which powerfully confirms that the

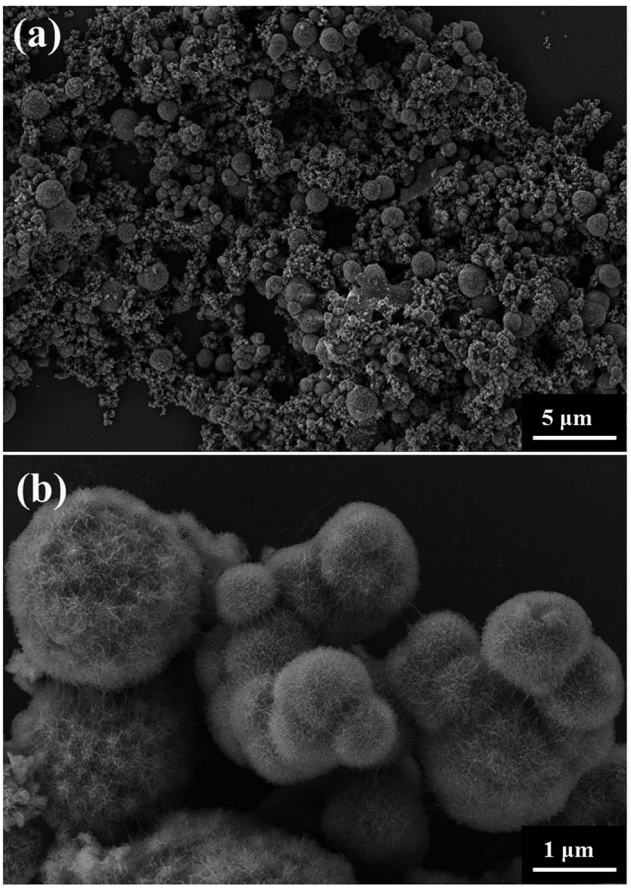

Fig. 5 SEM images of CP/LDH-7 composite with low (a) and high (b) magnifications.

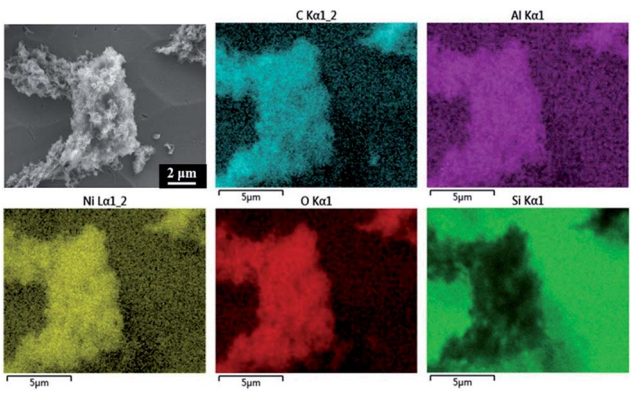

Fig. 6 SEM image of CP/LDH-5 and the corresponding EDS mapping of C (azure), Al (purple), Ni (yellow) and O (red) elements. The Si EDS mapping can be ascribed to the silicon wafer loading the CP/LDH-5 specimen.

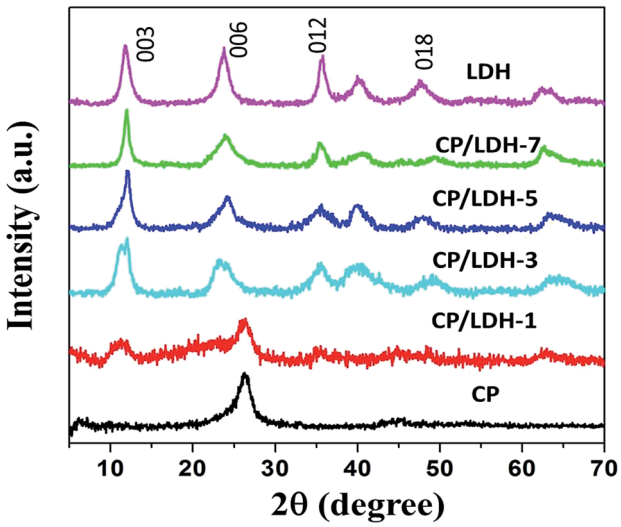

Fig. 7 XRD patterns of CP materials, CP/LDH hybrids with different contents of NiAl-LDH nanosheets, as well as pure NiAl-LDH spheres.

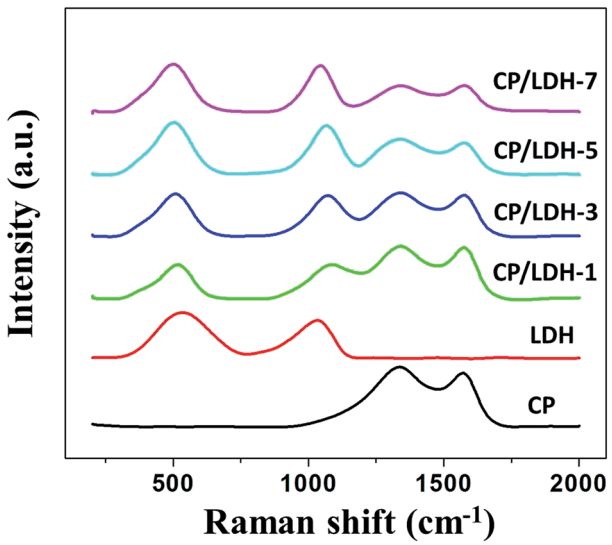

Fig. 8 Raman spectra of CPs, CP/LDH composites with different contents of NiAl-LDHs, as well as pure NiAl-LDH spheres.

quasi-reversible and continuous Faradic redox reactions of NiAl-LDHs during the charging/discharging process that contributed pseudo-capacitance to the CP/LDH-5 composite electrode.[12,50] In addition, the cathodic and anodic peaks in the CV curves of CP/LDH-5 exhibit only a small shift toward negative and positive potentials with the scan rate increasing. The nearly linear increase of the redox peak currents proves that the electrode reaction corresponds to the quasi-reversible and diffusion-controlled process,[13,51] which is crucial to their pseudo-capacitance. Specific capacitances of CP materials, pure NiAl-LDH spheres, and CP/LDH hybrids at different scan rates were calculated from CVs curves according to eqn (1) as presented in Fig. 9d. Obviously, CP/LDH hybrids show enhanced specific capacitance compared to that of CP materials and pure NiAl-LDH spheres, which confirms the combined effect of the EDLC performance of CP materials and pseudo-capacitance of the surface located NiAl-LDH nanosheets. Moreover, the maximum specific capacitance of CP/LDH-5 reaches 1355 F g^{-1} at 5 mV s^{-1}, and maintain at 857 F g^{-1} when the scan rate is up to 100 mV s^{-1}, indicating the excellent rate performances of CP/LDH

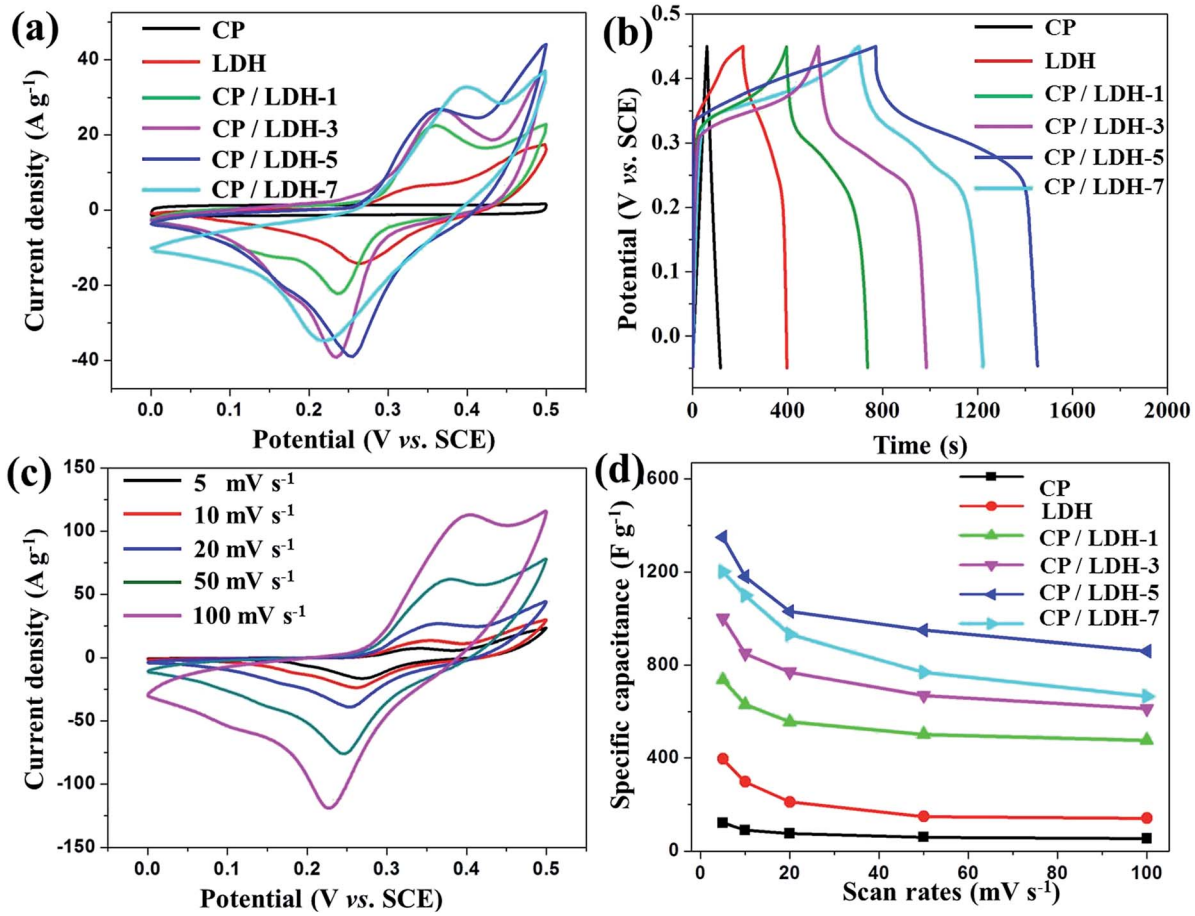

Fig. 9 CV curves of CP material, pure NiAl-LDH sphere, and CP/LDH hybrids with different contents of NiAl-LDHs at 20 mV s^{-1} (a); galvanostatic charge–discharge curves at 1 A g^{-1} (b); CV curves of CP/LDH-5 at various scan rates from 5 to 100 mV s^{-1} (c); specific capacitance of CP materials, pure NiAl-LDH spheres, and CP/LDH hybrids at different scan rates (d).

hybrids. In order to thoroughly understand the capacitive effect of outer layer of NiAl-LDHs, ICP analysis of CP/LDH-5 sample was performed, and the metal ions of Al^{3+} and Ni^{2+} were about 19.8 mg L^{-1} and 53.5 mg L^{-1} respectively in the diluted acid solutions (as seen in Table S1†), with a mass ratio of 0.37 : 1. The high electrochemical performance of CP/LDH-5 can be ascribed to the excellent capacitive performance of Ni hydroxide, as well as the doping effect of Al element.[15,39] However, with the scan rates increasing, the specific capacitance of the prepared samples gradually decreased, which can be ascribed to the reason that the movement of ions and protons are limited by the diffusion at high scan rates, and only the outer active sites can be utilized for charge storage during the charging/discharging process.[52–54] Also, non-activated CP materials located with same content of NiAl-LDHs as CP/LDH-5 sample have been prepared and used as electrode materials, as seen in Fig. S2.† CV curves show weaker current densities as well as shorter discharge time compared with that of CP/LDH-5, resulting in a specific capacitance of 730 F g^{-1} which is much lower than 1355 F g^{-1} of CP/LDH-5. These results clearly confirm the activation effect of KOH, and the resulted porous structures can play an important role in enhancing the electrochemical properties of CP/LDH composites.

EIS analysis was further employed in the frequency range of 100 kHz to 0.01 Hz with an ac perturbation of 10 mV to understand the difference among the fundamental electrochemical behaviors of CP materials, pure NiAl-LDH spheres, and CP/LDH hybrids (Fig. 10a). The corresponding equivalent circuit for the EIS spectra was provided in Fig. 10b. Interestingly, no semicircle can be observed in the EIS spectra of CP material in the high frequencies due to the good conductivity. The EIS plots of CP/LDH hybrids show smaller semicircle in the high frequency range compared to that of pure NiAl-LDH spheres, indicating lower charge transfer resistance (R_F) than pure NiAl-LDHs.[46,58] Moreover, the more vertical lines in low frequencies region of CP/LDH hybrids than that of pure NiAl-LDH spheres indicates better capacitive behaviors and lower diffusion resistance of ions.[55–57] The magnitude of equivalent series resistance (R_S) can be obtained from the *x*-intercept of the Nyquist plot at real part Z' in the high frequencies range, which represents the combined resistance from the ionic resistance of the electrolyte, intrinsic resistance of the electrodes, and contact resistance at the electrode/current collector interface.[59,60] Here, R_s of CP materials, CP/LDH-5 hybrid, and pure NiAl-LDH spheres is observed to be about 1.9 Ω, 2.1 Ω and 4.0 Ω, respectively. This further indicates that the prepared CP/LDH hybrids have much lower charge-

transfer resistance and ion diffusion resistance than pure NiAl-LDH spheres, thus resulting in higher reactivity and faster reaction kinetics. Hence, it can be concluded that the successful hybridization of NiAl-LDH nanosheets with CP materials have achieved efficient synergistic effect of capacitance improvement.

Long cycle life of the electrode materials is also an important requirement for their practical applications. In this work, cyclic performances of CP materials, pure NiAl-LDH spheres, and CP/LDH-5 hybrid electrodes were examined by galvanostatic charge/discharge tests for 2000 cycles, as shown in Fig. 11a. CP/LDH-5 hybrids show remarkably enhanced cyclic stability (90% retained) compared with the corresponding pure NiAl-LDH spheres (55% retained) after 2000 cycles, indicating the superior long-term cycle stability of CP/LDH hybrids. The good cycling stability and long lifetime of CP/LDH-5 hybrids can be further confirmed by the similar potential-time response behavior during each charging/discharging cycle (Fig. 11b). This excellent cycling performance of CP/LDH hybrids can be ascribed to the reason that porous structure of CP material ensures fast adsorption/desorption of ions and makes full use of the located NiAl-LDH nanosheets. To our interesting, the specific capacitance of CP/LDH-5 hybrids unexpectedly increased after the initial stage and achieved the maximum value of 1387 F g^{-1} after 200 cycles. This result can be ascribed to the efficient activation process where the unused electrochemically active Ni sites of

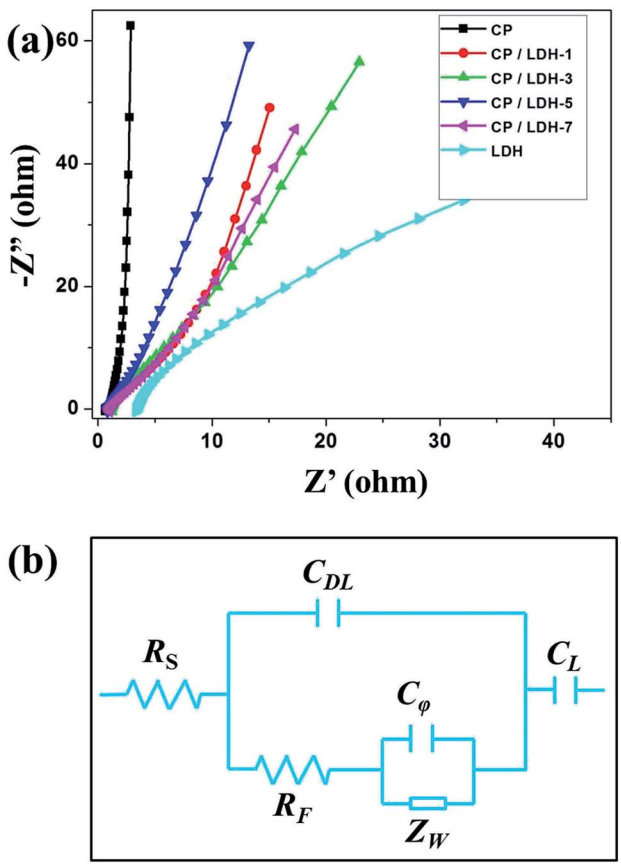

Fig. 10 Nyquist plots of CP materials, pure NiAl-LDH spheres, and CP/LDH hybrids (a); electrical equivalent circuit for fitting the impedance spectra of CP materials, NiAl-LDH spheres, and CP/LDH hybrids (b).

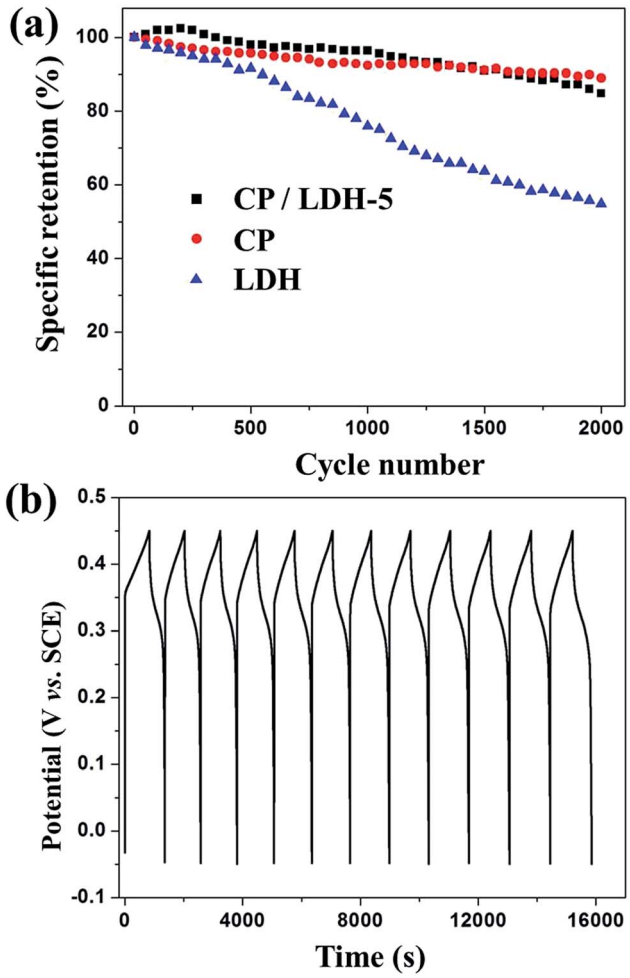

Fig. 11 Cycling stability of CP materials, pure NiAl-LDH spheres and CP/LDH-5 hybrid upon charging/discharging at a current density of 1 A g^{-1} (a); galvanostatic charge/discharge curves of CP/LDH-5 hybrid (b).

NiAl-LDH nanosheets at the initial stage can be fully exposed to the electrolyte after repetitive charging/discharging cycles,[50,61–63] thus resulting in the exciting increase of the specific capacitance of CP/LDH-5 hybrid. In addition, important parameters of energy density (E) and power density (P) of CP/LDH-5 sample have been calculated based on the charge–discharge curves (as seen in Fig. S3†) and further used to characterize its capacitive behaviors. Fig. S4† shows the ragone plots of CP/LDH-5, and the energy density reduces slowly with the increase of power density. The maximum energy density of 86.1 W h kg^{-1} (with a power density of 499 W kg^{-1}) and power density of 6.72 kW kg^{-1} (with energy density of 54.1 W h kg^{-1}) were achieved, which are comparable with the previously reported results based on active electrode materials, further illustrating good capacitive behavior of these layered NiAl-LDHs hybridized with porous CP materials.

4. Conclusions

In this work, carbon nanoparticles with mesoporous structure and high specific surface area have been facilely and eco-friendly prepared from the fallen ginkgo leaves *via* milling

and chemical activation. NiAl-LDH nanosheets have been homogeneously deposited on the surface of CPs which act as supporting frameworks, achieving the fabrication of CP/LDH hybrids. By adjusting the amount of precursors, CP/LDH hybrids with different contents of NiAl-LDHs were prepared. Electrochemical characterizations show that the CP/LDH hybrids exhibit much better capacitance performance than the CPs and pure NiAl-LDHs when used as electrode materials in supercapacitors. This enhanced electrochemical performance of CP/LDH hybrids can be ascribed to the synergistic effect of the EDLC effect from CPs and pseudocapacitance contribution from NiAl-LDHs by forming the hierarchical porous-layer structures. Therefore, the hierarchically nanostructured CP/LDH hybrid electrodes with excellent electrochemical performance and low cost as well as simple preparation process may find potential applications in energy storage and conversion devices.

Acknowledgements

The authors are grateful for the financial support from the National Natural Science Foundation of China (51125011, 51433001).

Notes and references

1 L. Zhao, L. Fan, M. Zhou, H. Guan, S. Qiao, M. Antonietti and M. Titirici, *Adv. Mater.*, 2010, **22**, 5202–5206.
2 A. S. Arico, P. Bruce, B. Scrosati, J. M. Tarascon and W. van Schalkwijk, *Nat. Mater.*, 2005, **4**, 366–377.
3 L. Chen, X. Zhang, H. Liang, M. Kong, Q. Guan, P. Chen, Z. Wu and S. Yu, *ACS Nano*, 2012, **6**, 7092–7102.
4 J. Xu, S. Gai, F. He, N. Niu, P. Gao, Y. Chen and P. Yang, *J. Mater. Chem. A*, 2014, **2**, 1022–1031.
5 Q. Wu, Y. X. Xu, Z. Y. Yao, A. R. Liu and G. Q. Shi, *ACS Nano*, 2010, **4**, 1963–1970.
6 Z. J. Fan, J. Yan, L. J. Zhi, Q. Zhang, T. Wei, J. Feng, M. L. Zhang, W. Z. Qian and F. Wei, *Adv. Mater.*, 2010, **22**, 3723–3728.
7 A. Lewandowski, A. Olejniczak, M. Galinski and I. Stepniak, *J. Power Sources*, 2010, **195**, 5814–5819.
8 X. Lang, A. Hirata, T. Fujita and M. Chen, *Nat. Nanotechnol.*, 2011, **6**, 232–236.
9 Z. Fan, J. Yan, T. Wei, L. Zhi, G. Ning, T. Li and F. Wei, *Adv. Funct. Mater.*, 2011, **21**, 2366–2375.
10 X. Zhao, L. Zhang, S. Murali, M. D. Stoller, Q. Zhang, Y. Zhu and R. S. Ruoff, *ACS Nano*, 2012, **6**, 5404–5412.
11 Y. Li, X. Zhao, P. Yu and Q. Zhang, *Langmuir*, 2013, **29**, 493–500.
12 H. Jiang, P. S. Lee and C. Li, *Energy Environ. Sci.*, 2012, **6**, 41–53.
13 H. Jiang, J. Ma and C. Li, *Adv. Mater.*, 2012, **24**, 4197–4202.
14 Z. Zhu, Y. Hu, H. Jiang and C. Li, *J. Power Sources*, 2014, **246**, 402–408.
15 W. Yang, Z. Gao, J. Wang, J. Ma, M. Zhang and L. Liu, *ACS Appl. Mater. Interfaces*, 2013, **5**, 5443–5454.
16 Y. Zhai, Y. Dou, D. Zhao, P. F. Fulvio, R. T. Mayes and S. Dai, *Adv. Mater.*, 2011, **23**, 4828–4850.
17 Z. Wen, X. Wang, S. Mao, Z. Bo, H. Kim, S. Cui, G. Lu, X. Feng and J. Chen, *Adv. Mater.*, 2012, **24**, 5610–5616.
18 L. Dai, D. W. Chang, J. B. Baek and W. Lu, *Small*, 2012, **8**, 1130–1166.
19 X. Zhao, H. Tian, M. Zhu, K. Tian, J. J. Wang, F. Kang and R. A. Outlaw, *J. Power Sources*, 2009, **194**, 1208–1212.
20 L. L. Zhang and X. S. Zhao, *Chem. Soc. Rev.*, 2009, **38**, 2520–2531.
21 P. Kleszyk, P. Ratajczak, P. Skowron, J. Jagiello, Q. Abbas, E. Frąckowiak and F. Béguin, *Carbon*, 2015, **81**, 148–157.
22 A. Jain and S. K. Tripathi, *J. Solid State Electrochem.*, 2013, **17**, 2545–2550.
23 J. Gamby, P. L. Taberna, P. Simon, J. F. Fauvarque and M. Chesneau, *J. Power Sources*, 2001, **101**, 109–116.
24 S. Wang, Z. Ren, J. Li, Y. Ren, L. Zhao and J. Yu, *RSC Adv.*, 2014, **4**, 31300–31307.
25 M. Biswal, A. Banerjee, M. Deo and S. Ogale, *Energy Environ. Sci.*, 2013, **6**, 1249–1259.
26 L. Zhang, F. Zhang, X. Yang, K. Leng, Y. Huang and Y. Chen, *Small*, 2013, **9**, 1342–1347.
27 C. Wu and Y. Xie, *Energy Environ. Sci.*, 2010, **3**, 1191–1206.
28 D. G. Evans and X. Duan, *Chem. Commun.*, 2006, **46**, 485–496.
29 J. Feng, X. Sun, C. Wu, L. Peng, C. Lin, S. Hu, J. Yang and Y. Xie, *J. Am. Chem. Soc.*, 2011, **133**, 17832–17838.
30 S. Huang, G. N. Zhu, C. Zhang, W. W. Tjiu, Y. Y. Xia and T. X. Liu, *ACS Appl. Mater. Interfaces*, 2012, **4**, 2242–2249.
31 F. Zhang, L. Zhao, H. Chen, S. Xu, D. G. Evans and X. Duan, *Angew. Chem., Int. Ed.*, 2008, **47**, 2466–2469.
32 J. Huang, T. Lei, X. Wei, X. Liu, T. Liu, D. Cao, J. Yin and G. Wang, *J. Power Sources*, 2013, **232**, 370–375.
33 Z. Lu, W. Zhu, X. Lei, G. R. Williams, D. O'Hare, Z. Chang, X. Sun and X. Duan, *Nanoscale*, 2012, **4**, 3640–3643.
34 V. Gupta, S. Gupta and N. Miura, *J. Power Sources*, 2009, **189**, 1292–1295.
35 J. Wang, Y. Song, Z. Li, Q. Liu, J. Zhou, X. Jing, M. Zhang and Z. Jiang, *Energy Fuels*, 2010, **24**, 6463–6467.
36 J. Memon, J. Sun, D. Meng, W. Ouyang, M. A. Memon, Y. Huang, S. Yan and J. Geng, *J. Mater. Chem. A*, 2014, **2**, 5060–5067.
37 Y. Zhao, S. He, M. Wei, D. G. Evans and X. Duan, *Chem. Commun.*, 2010, **46**, 3031–3033.
38 S. Yang, K. Chang, Y. Huang, Y. Lee, H. Tien, S. Li, Y. Lee, C. Liu, C. M. Ma and C. Hu, *Electrochem. Commun.*, 2012, **14**, 39–42.
39 R. Wang, P. Wang, X. Yan, J. Lang, C. Peng and Q. Xue, *ACS Appl. Mater. Interfaces*, 2012, **4**, 5800–5806.
40 J. Górka, A. Zawislak, J. Choma and M. Jaroniec, *Carbon*, 2008, **46**, 1159–1161.
41 J. Gong, T. Liu, X. Wang, X. Hu and L. Zhang, *Environ. Sci. Technol.*, 2011, **45**, 6181–6187.
42 A. Malak-Polaczyk, C. Vix-Guterl and E. Frackowiak, *Energy Fuels*, 2010, **24**, 3346–3351.
43 Y. L. Niu, R. Y. Li, Z. J. Li, Y. J. Fang and J. K. Liu, *Electrochim. Acta*, 2013, **94**, 360–366.

44 J. Zhao, L. Yang, F. Li, R. Yu and C. Jin, *Carbon*, 2009, **47**, 744–751.
45 Y. Ou, C. Peng, J. Lang, D. Zhu and X. Yan, *New Res. Carbon Mater.*, 2014, **29**, 209–215.
46 P. Simon and Y. Gogotsi, *Nat. Mater.*, 2008, **7**, 845–854.
47 Z. Liu, R. Ma, M. Osada, N. Iyi, Y. Ebina, K. Takada and T. Sasaki, *J. Am. Chem. Soc.*, 2006, **128**, 4872–4880.
48 H. Li, R. Liu, D. Zhao and Y. Xia, *Carbon*, 2007, **45**, 2628–2635.
49 L. Zhang, J. Wang, J. Zhu, X. Zhang, K. San Hui and K. N. Hui, *J. Mater. Chem. A*, 2013, **1**, 9046–9053.
50 G. Wang, J. Huang, S. Chen, Y. Gao and D. Cao, *J. Power Sources*, 2011, **196**, 5756–5760.
51 Y. Lin, L. Ruiyi, L. Zaijun, L. Junkang, F. Yinjun, W. Guangli and G. Zhiguo, *Electrochim. Acta*, 2013, **95**, 146–154.
52 L. Wang, D. Wang, X. Y. Dong, Z. J. Zhang, X. F. Pei, X. J. Chen, B. Chen and J. Jin, *Chem. Commun.*, 2011, **47**, 3556–3558.
53 E. Géraud, S. Rafqah, M. Sarakha, C. Forano, V. Prevot and F. Leroux, *Chem. Mater.*, 2008, **20**, 1116–1125.
54 T. Stimpfling and F. Leroux, *Chem. Mater.*, 2010, **22**, 974–987.
55 Y. Wang, Z. Q. Shi, Y. Huang, Y. F. Ma, C. Y. Wang, M. M. Chen and Y. S. Chen, *J. Phys. Chem. C*, 2009, **113**, 13103–13107.
56 W. Chen, T. Wen and H. Teng, *Electrochim. Acta*, 2003, **48**, 641–649.
57 J. Han, L. L. Zhang, S. Lee, J. Oh, K. Lee, J. R. Potts, J. Ji, X. Zhao, R. S. Ruoff and S. Park, *ACS Nano*, 2013, **7**, 19–26.
58 J. Xu, Y. Dong, J. Cao, B. Guo, W. Wang and Z. Chen, *Electrochim. Acta*, 2013, **114**, 76–82.
59 M. K. Liu, W. W. Tjiu, J. S. Pan, C. Zhang, W. Gao and T. X. Liu, *Nanoscale*, 2014, **6**, 4233–4242.
60 J. Yan, Z. Fan, T. Wei, W. Qian, M. Zhang and F. Wei, *Carbon*, 2010, **48**, 3825–3833.
61 X. Zhang, W. Shi, J. Zhu, W. Zhao, J. Ma, S. Mhaisalkar, T. L. Maria, Y. Yang, H. Zhang, H. H. Hng and Q. Yan, *Nano Res.*, 2010, **3**, 643–652.
62 B. K. Gupta, P. Thanikaivelan, T. N. Narayanan, L. Song, W. Gao, T. Hayashi, A. Leela Mohana Reddy, A. Saha, V. Shanker, M. Endo, A. A. Martí and P. M. Ajayan, *Nano Lett.*, 2011, **11**, 5227–5233.
63 Z. Gao, J. Wang, Z. Li, W. Yang, B. Wang, M. Hou, Y. He, Q. Liu, T. Mann, P. Yang, M. Zhang and L. Liu, *Chem. Mater.*, 2011, **23**, 3509–3516.